JOURNAL OF MATERIALS SCIENCE 27 (1992) 1575–1584

Liquid-phase sintering in the glass–cordierite system

JAU-HO JEAN, T. K. GUPTA
Alcoa Electronic Packaging, Inc. Alcoa Technical Center, Alcoa Center, PA 15069, USA

Densification mechanisms and kinetics of liquid-phase sintering were studied using borosilicate glass–cordierite as a model system. It is shown that the sintering behaviour can be represented predominantly by a non-reactive liquid-phase sintering and that the densification is achieved mainly in the initial stage of sintering. From the activation energy estimates of densification, it is concluded that the predominant mechanism of densification is the viscous flow of glass with contribution arising from both viscous sintering of glass and glass redistribution kinetics. The latter evidence stems from the microstructural observation that as the sintering proceeds, the glass undergoes a time-dependent wetting behaviour. Based on this observation, and calculated infiltration times of melt into the porous compact, it is found that the time-dependent contact angle between the melt and the solid particles plays a significant role in the glass redistribution process.

1. Introduction

Liquid-phase sintering has been phenomenologically classified into three stages, including particle rearrangement, solution and precipitation, and solid state sintering with the formation of a skeleton [1]. In the first stage, densification occurs rapidly as soon as the liquid phase is formed. Pores are filled through liquid-phase redistribution, and the particles are rearranged due to capillary pressure, resulting in a closer packing. In general, the densification occurring in the first stage is the most rapid during liquid-phase sintering. In the second stage, the densification mainly takes place through particle-morphology accommodation, in which the small particles dissolve and precipitate on the larger particles. The characteristic features of this stage are particle disintegration [2], directional grain growth [3], normal grain growth, and grain-shape accommodation [4]. In the last stage, the densification kinetics are very slow because a rigid skeleton is formed. A typical phenomenon occurring in the last stage is a significant grain growth through Ostwald ripening kinetics [5]. Because the experimental results of this research show that the densification mainly occurs in the first stage of liquid-phase sintering, a brief summary of theories and previous studies on the first stage of liquid-phase sintering is given below.

The first stage of liquid-phase sintering can be further divided in three steps: melt formation, melt redistribution and particle rearrangement [6]. For the system without dissolution taking place during liquid-phase sintering, the densification is mainly achieved in this stage. Typical systems are W–Cu [7, 8], W–Ag [7], and Al_2O_3–glass [9], in which the components are practically insoluble in each other. The liquid-phase sintering kinetics of insoluble systems is referred to as non-reactive liquid-phase sintering (NLPS) [10].

When the melt viscosity is low, e.g. copper ($< 5 \times 10^{-3}$ N s m^{-2}) in W + Cu where the melt formation takes place in a very short period of time, the melt-formation kinetics is not a rate-controlling step during liquid-phase sintering. However, the melt-formation step can be very slow if the viscosity of melt is high ($> 10^5$ N s m^{-2}), as is observed in the glass–ceramics system where on heating, the glass powders gradually melt and coalesce through viscous sintering. As this melt redistributes into the porous compacts, the important rate-controlling factors include the viscosity of melt, the contact angle of melt on the refractory particles, the surface tension of melt, the pore size of green compact and the melt content. When a liquid bridge forms between particles, a local rearrangement force, composed of surface tension acting at the wetting particle surface and capillary pressure, is operative at the solid/liquid interface [7]. The rearrangement force can be attractive if the liquid wets the powder, or repulsive if the liquid is non-wetting. The magnitude of the rearrangement force is a function of particle size, pore size, wetting angle, particle morphology and liquid phase content. Theoretical calculations show that with a wetting liquid the rearrangement force becomes greater with less liquid phase content for spherical powders [11], but increases with increasing liquid phase content for irregular powders [12]. A larger shrinkage can be expected with a greater rearrangement force, which has been experimentally confirmed by using copper-coated tungsten powders [13].

The rate-controlling step during NLPS can be obtained by comparing the calculated activation energy of densification with the activation energy of melt flow. If these values are comparable, the densification is considered to be controlled by viscous flow of melt,

0022–2461

either melt formation or melt redistribution. Otherwise, the particles rearrangement process is the rate-limiting step during NLPS. For example, in W–Cu [8] the rate-limiting process is particle rearrangement, because the activation energy of densification, $120–210 \times 10^3$ J mol^{-1}, is much larger than that of viscous flow of copper melt, 330 J mol^{-1}, at temperatures ranging from 1100–1600 °C [14]. In addition, the contact angle decreases from 40° at 1100 °C to 0° at 1350 °C [15], which increases the rearrangement force by at least two-fold [7]. This can increase the densification rate dramatically.

To obtain full density by NLPS, a sufficient quantity of liquid phase is required. Several values have been suggested by different research groups, e.g. 25 vol % by Cannon and Lenel [1], 35 vol % for spherical powders by Kingery [16], 50 vol % for irregular powders by Eremenko *et al.* [7], and 26 vol % for monosize spherical powders by Kwon [17]. However, no experimental results confirmed any of the above suggested liquid phase contents. This is probably because the critical glass content is determined by too many variables, such as particle morphology, particle size ratio, particle size distribution, packing density, mixing uniformity, viscosity of the liquid phase, and the contact angle of melt on refractory powder, which are very difficult to control altogether. Actually, very few insoluble systems have been densified to greater than 95% relative density, except the W–Cu system reported by Sebastian and Tendolkar [8]. It is found that a high sintered density, > 97%, can be obtained with 40 vol % Cu at 1300 °C by using co-reduced powders, in which very fine and homogeneous mixing powders are obtained. In contrast, a low sintered density, 70%, is obtained at the same conditions by using co-mixed tungsten and copper powders.

This research was undertaken to understand the densification mechanisms and kinetics of glass-filled ceramics using glass–cordierite as a model system. The effects of glass content, and sintering temperature were studied. The rate-limiting step during densification was determined from apparent activation energy calculations, microstructural observation and melt redistribution kinetics.

2. Experimental procedure

2.1. Materials

The borosilicate glass used in this study has an approximate composition of 75 wt % SiO_2 and 25 wt % B_2O_3. Particle size distributions of the borosilicate glass and cordierite powders used in this study were determined by sedimentation. The crystallinity of these as-received powders was determined by XRD analysis and specific surface area was measured by the nitrogen-BET method.

2.2. Viscosity of borosilicate glass

The viscosity of glass was measured by a fibre elongation method. For viscosity measurement, the glass was melted at temperatures above 1300 °C, then 0.5 mm diameter glass fibres were drawn in air.

2.3. Contact angle of borosilicate glass

The contact angles of borosilicate glass were measured as a function of temperature on > 99% dense cordierite substrates made by hot isostatic pressing. The samples were sectioned and polished down to a 0.25 μm finish using diamond paste. Prior to the contact angle measurement, the substrate was cleaned using trichlorethane and acetone in a sonicator for 10 min each. The unground glass powder was placed on the cordierite substrate and fired in air at a heating rate of 50 °C min^{-1} to the predetermined temperatures, corresponding to sintering temperatures. The contact angles were measured after firing at the set temperature for 120 min by using a telegoniometer.

2.4. Sample preparation for sintering

Powders and 5 wt % polyethylene glycol binder were mixed in 1-propanol. The slurry was deagglomerated by a high-energy ultrasonic horn. Mixing was continued using a Turbula mixer for 2 h. The powder mixture was dried, ground and uniaxially pressed at about 9×10^6 N m^{-2} to make pellets 1.9 cm diameter and 0.3 cm high. Green densities of the pressed samples were measured dimensionally and used to determine densification behaviour. The temperature for the binder burnout was determined by thermogravimetric analysis (TGA), at a heating rate of 5 °C min^{-1} in air. The TGA results show that the major weight loss occurs at temperatures from 250–350 °C, and no appreciable weight loss is observed above 400 °C. Therefore, binder was removed by firing the samples in flowing air at 5 °C min^{-1} from room temperature to 500 °C. To remove organic binder completely, the temperature was held at 500 °C for 60 min. A small decrease in green density, < 2%, was observed after binder burnout. Samples fired at 500 °C for 60 min were used to determine the pore-size distributions of green compacts by mercury porosimetry.

2.5. Sintering

Samples were sintered isothermally in air at temperatures ranging from 800–900 °C. Samples were pushed into the heating zone after binder burnout. A period of 2 min was allowed for the samples to equilibrate at the sintering temperatures. After completion of sintering, samples were air-quenched to room temperature. No cracks were visually observed.

2.6. Sintered density measurement

The sintered densities were determined by the water displacement method, i.e. Archimedes' method. Samples were immersed in water, and the open pores were filled with water in vacuum for 2 h. The theoretical densities, 2.16 g cm^{-3} for the glass and 2.55 g cm^{-3} for the cordierite, were used to estimate the theoretical densities of borosilicate glass-filled cordierite compacts by using the rule of mixture. The sintered densities were qualitatively confirmed by microstructural observations. The reported densities are the average of three samples.

2.7. Microstructural observations

To reveal the cordierite grain size and morphology, the polished samples were heavily etched with 10 wt % HCl aqueous solution. Grain sizes were determined from scanning electron micrographs by the intercept method. To examine the microstructural changes during firing, scanning electron micrographs of fracture surfaces were taken for the samples fired at different temperatures for various times.

3. Results

3.1. Powder and green compact characterization

Scanning electron micrographs of the ground borosilicate and cordierite powders show that the powders are irregular and have a size range of 0.3–6 μm for borosilicate and 0.5–10 μm for cordierite. These size ranges are very close to those measured by sedimentation. The particle size distributions measured by sedimentation show that the powders have a median size of 1.9 μm for glass and 4.1 μm for cordierite. Specific surface areas determined by BET were 7.4 $m^2 g^{-1}$ for glass, and 1.2 $m^2 g^{-1}$ for cordierite, which are close to the geometric surface areas calculated based upon the assumptions of monosized and spherical powders. This indicates that the powders are not porous. The measured green densities were in the range 59%–61% theoretical densities. The pore size distribution of the green compacts, fired at 500 °C for 60 min, ranged from 0.3–2 μm and had a median pore radius of 0.265 μm.

3.2. Viscosity and contact angle measurement

Experimental results for glass viscosity are shown in Fig. 1. As indicated in the figure, the glass has an annealing point of 508 °C and a softening point of 793 °C. A linear relation between log viscosity and $1/T$ with an activation energy of 290–310 kJ mol^{-1}, determined by the least-squares fit method, is obtained and can be described with the following equation

$$\eta = 10^{-7} \exp(300 \times 10^3/RT) \quad (1)$$

Using Equation 1 the extrapolated viscosities at different temperatures were calculated and are listed in Table I. The contact angles measured at various temperatures are also shown in Table I. No significant change in contact angle with temperatures from 800–900 °C was observed.

3.3. Densification

The densification behaviour is shown as densification factor versus time. The densification factor (DF), which is equal to the fraction of porosity eliminated as suggested by Cannon and Lenel [1], is defined by the following equation

$$DF = (D_t - D_g)/(D_{th} - D_g) \quad (2)$$

where D_t is the sintered density at any time, D_g the green density of the as-pressed compact, and D_{th} the theoretical density calculated by the mixing rule. Although the green density of the compacts after binder burnout should be used in Equation 2, there is difficulty in obtaining the reliable densitites of the compacts because of their fragility, and hence we used the density of the as-pressed samples. A typical plot showing the densification factor as a function of time at the glass content indicated is illustrated in Fig. 2. For the systems with < 30 vol % glass, a negative densification factor is observed in the first several minutes.

TABLE I Viscosity and contact angle of borosilicate glass as a function of temperature

	Temperature (°C)				
	800	825	850	875	900
η (10^5 N s m^{-2})	29.0	14.0	6.6	3.3	1.76
θ (deg)	34.5	33.2	32.0	34.1	27.2

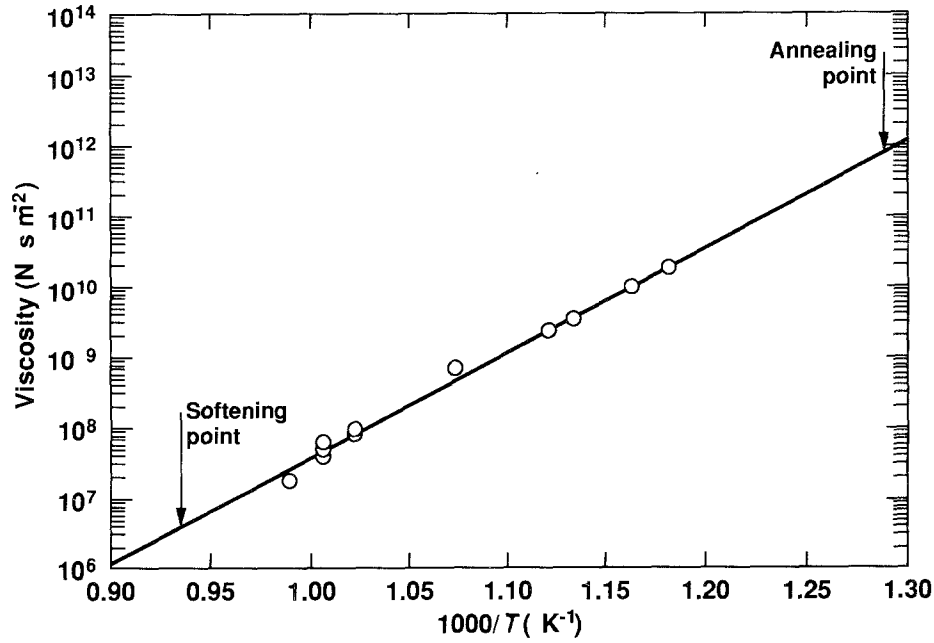

Figure 1 Viscosity of borosilicate glass at various temperatures.

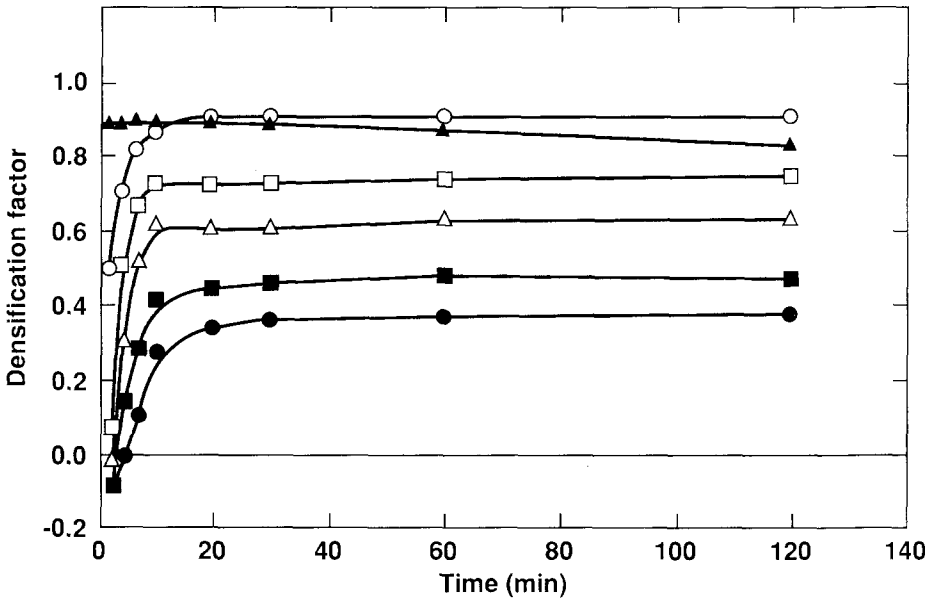

Figure 2 Densification factor versus time at 850 °C for various glass contents (vol %): (●) 20, (■) 30, (△) 40, (□) 50, (○) 60, (▲) 100.

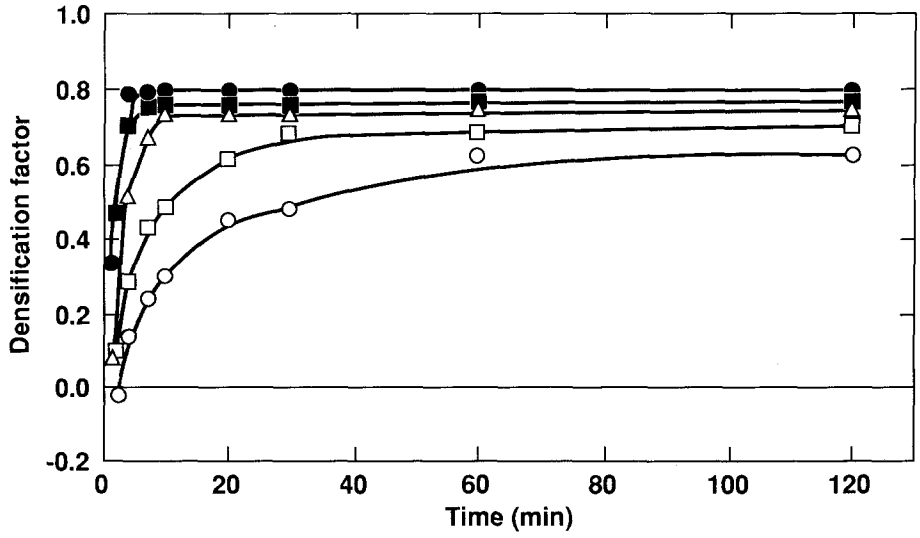

Figure 3 Densification factor versus time at various temperatures for 50 vol % borosilicate glass–50 vol % cordierite. (○) 800, (□) 825, (△) 850, (■) 875, (●) 900 °C.

This result is due to the fact that the green density of as-pressed compact, which was used to calculate DF, is reduced by a factor of 2% after binder burnout. This phenomenon is especially evident when firing is conducted at temperatures less than 850 °C. In Fig. 2 the densification takes place rapidly in the first 10 min, then slows down, and eventually stops at a constant densification factor. Pure borosilicate glass reaches a high densification factor of 0.9 almost instantly (< 2 min); however, because of bloating the densification factor decreases as the sintering continues, as shown in Fig. 2. The time needed to reach the constant densification factor can be determined from the intersection of two arbitrarily selected slopes, one from the constant densification factor and the other from the rising part of the densification factor versus time curve. It is found that the required period of time shows a negligible decrease with an increase in glass content ranging from 20–60 vol % at 850 °C. The same phenomenon is also observed at other temperatures from 800–900 °C. In contrary, the effect of temperature on the time needed to reach a constant densification factor is much more significant, as shown in Fig. 3. The time to reach a constant densification factor as a function of temperatures at various glass contents are tabulated in Table III under the heading of measured value, and will be discussed later. Fig. 4 presents a plot of the constant densification factor versus glass content at various temperature, showing that the data can be represented by straight lines. A similar result is also observed when the constant densification factor is plotted against temperature at a given glass content, as shown in Fig. 5.

4. Discussion

4.1. Densification mechanism

The linear relations presented in Figs 4 and 5 strongly suggest that the densification is very sensitive to the

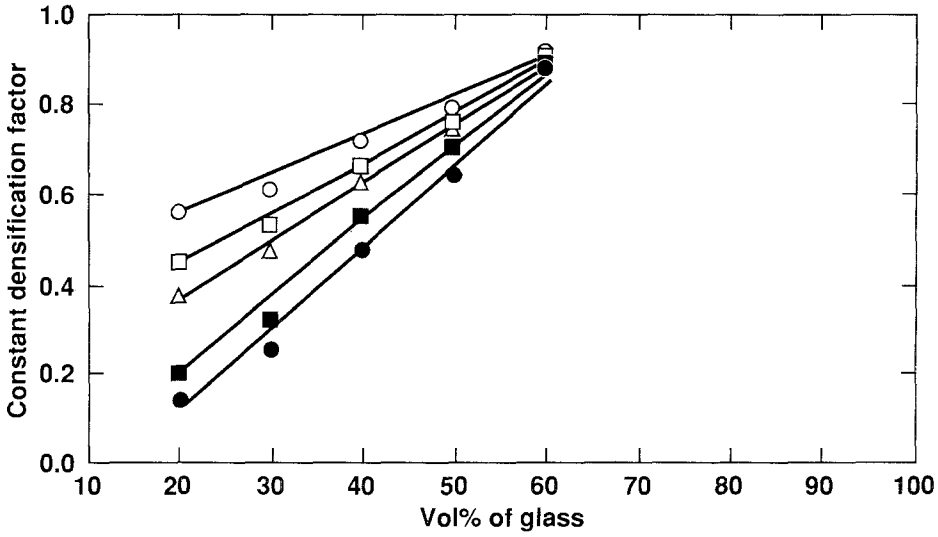

Figure 4 Constant densification factor versus glass content at various temperatures: (●) 800, (■) 825, (△) 850, (□) 875, (○) 900 °C.

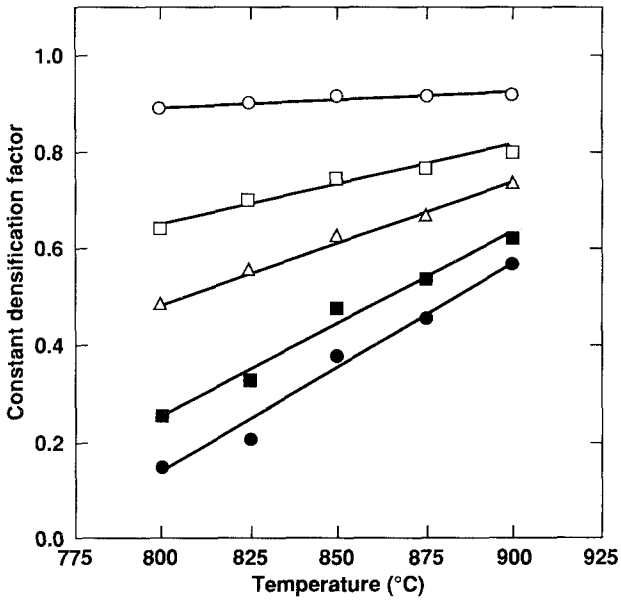

Figure 5 Constant densification factor versus temperature for various glass contents (vol %): (●) 20, (■) 30, (△) 40, (□) 50, (○) 60.

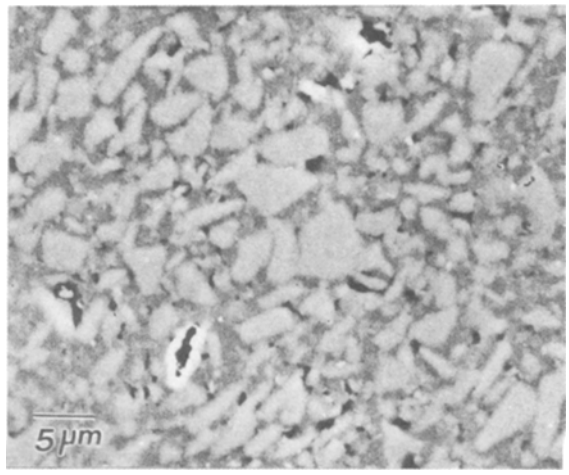

Figure 6 Microstructure of 50 vol % borosilicate glass and 50 vol % cordierite sintered at 850 °C for 30 min.

amount of glass present and the sintering temperatures used. It is further noted from Fig. 4 that the slopes of the straight lines decrease with increasing sintering temperature, indicating that the densification is more sensitive to glass content at lower sintering temperature. The mild temperature dependence of densification is also indicated in Fig. 5 from the decreasing slopes with higher glass content. The slope nearly vanishes at 60 vol % glass in the temperature range 800–900 °C. Based on the results presented in Figs 4 and 5, it can be concluded that the densification is primarily controlled by the amount of glass present in the system. A high sintered density, > 97%, can always be ensured with a large enough glass content, i.e. 60 vol % glass in the present case.

Having thus established the role of glass in the densification, it is now appropriate to examine the microstructure of the system to evaluate the mechanism of densification. A typical optical micrograph for the sample fired at 850 °C for 30 min, which is longer than that needed to reach the constant densification factor at this temperature, 15–20 min, is shown in Fig. 6. It is interesting to note that the initial cordierite grain does not change its size and the corners remain sharp, indicating that little dissolution and precipitation take place during densification. Similar phenomena are also observed at other temperatures investigated. This observation was further substantiated by examining the cross-section of a borosilicate glass–cordierite diffusion couple, fired at 900 °C for 300 min, as illustrated in Fig. 7. It is seen that little interdiffusion or chemical reaction, detected by energy dispersive X-rays (EDX), takes place across the interface. All the experimental results given above indicate that little or no dissolution and precipitation occur before the densification factor reaches its plateau, and the densification of borosilicate glass-filled cordierite ceramics in this study is concluded to be achieved in the first stage of liquid-phase sintering, i.e. melt redistribution and particle rearrangement. Similar results were also observed in the alumina–glass system by Kingery *et al.* [9].

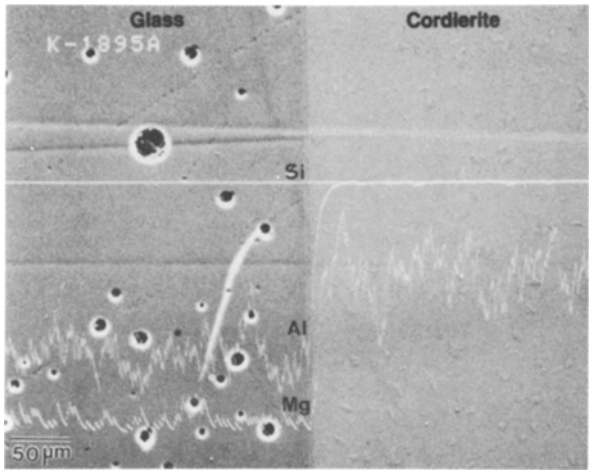

Figure 7 Cross-section of borosilicate glass-cordierite diffusion couple fired at 900 °C for 300 min, and concentration profiles of silicon, aluminium and magnesium.

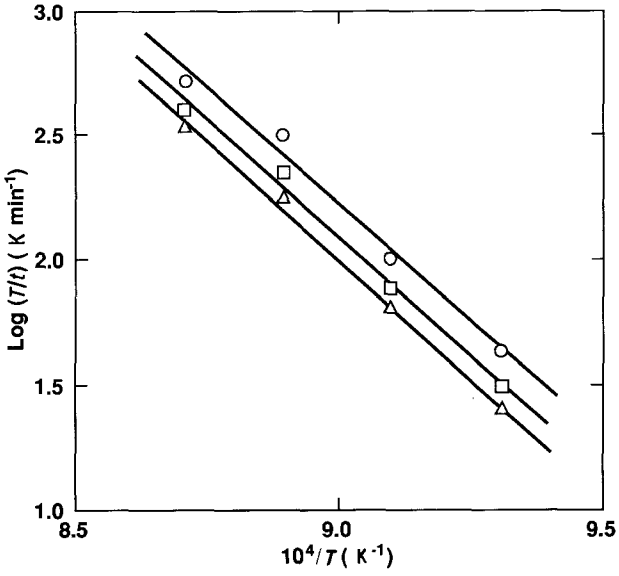

Figure 8 Apparent activation energy determination for 30 vol % glass and 70 vol % cordierite at various densification factors: (△) 0.20, (□) 0.15, (○) 0.10.

Since sintering is a thermally activated process in nature, the activation energy of the rate-controlling step can be determined from an Arrhenius plot. The plots are constructed using the logarithms of the specific rates T/t at a fixed densification factor versus $1/T$ [8], and the activation energy can be determined from the slopes by a least-squares fit method. From Fig. 8, the calculated apparent activation energies are 360 kJ mol^{-1} for DF = 0.1, 364 kJ mol^{-1} for DF = 0.15 and 372 kJ mol^{-1} for DF = 0.2 for the system with 30 vol % glass and 70 vol % cordierite. Table II lists all the apparent activation energies for the systems investigated at various densification factors. The apparent activation energies are in the range 330–390 kJ mol^{-1}; no significant difference is observed for the systems with glass content from 30–60 vol %. These apparent activation energies are close to the activation energy of viscous flow of borosilicate glass, 290–310 kJ mol^{-1}, determined from

TABLE II Apparent activation energy for the systems with various glass contents at different densification factors

DF	Apparent activation energy (kJ mol^{-1}) for glass contents of			
	60 vol %	50 vol %	40 vol %	30 vol %
0.70	389	–	–	–
0.65	368	–	–	–
0.60	343	–	–	–
0.50	–	376	–	–
0.45	–	368	–	–
0.40	–	385	347	–
0.35	–	364	343	–
0.30	–	–	335	–
0.25	–	–	330	–
0.20	–	–	–	360
0.15	–	–	–	364
0.10	–	–	–	372

Fig. 1. These results strongly suggest that the densification of borosilicate glass-filled cordierite ceramics at 800–900 °C is controlled by viscous flow of glass, either viscous sintering of glass or glass redistribution.

However, there are several observations which did not completely agree with viscous sintering of glass. First, a linear relation between linear shrinkage and time can be expected if the densification of the sintering of glass, based upon the classical viscous sintering theory by Frenkel [18]. This is not observed when the results shown in Figs 2 and 3 are replotted as linear shrinkage versus time, assuming an isotropic linear shrinkage. Secondly, according to glass-sintering theories proposed by Mackenzie and Shuttleworth [19], and Scherer [20], the densification behaviour of glass at different temperatures can be normalized by a parameter of reduced time, time/viscosity of glass. No such phenomenon is observed in this study using the viscosity data in Table I and the densification results in Fig. 3. It is, therefore, appropriate to consider the effect of cordierite on the melt-redistribution kinetics to interpret the present data.

4.2. Glass-redistribution kinetics

Because the glass-redistribution process during sintering is very similar to melt infiltration into a porous compact, the redistribution time can be estimated by using the following formula for calculating infiltration time [21]

$$x^2 = \frac{\gamma a \cos\theta_\infty t}{2\eta} \quad (3)$$

where x is the infiltration distance, γ is the surface tension of glass, a is the capillary radius, t is the time, θ_∞ is the equilibrium contact angle, and η is the viscosity of the glass. In Equation 3 the contact angle has been assumed to be time-independent, which fits the experimental conditions of contact-angle measurement with the glass powder described earlier. The time needed for borosilicate glass to infiltrate a porous

TABLE III Infiltration time of borosilicate glass calculated using Equation 3 for time-independent and Equation 6 for time-dependent contact angle, and the measured time periods needed to reach a constant densification factor at various temperatures

Temperature (°C)	Infiltration time (s)		
	Measured value	Equation 3	Equation 6
900	120– 240	1– 9	20– 140
875	420– 600	2–13	40– 270
850	900–1200	3–18	80– 540
825	1800–2400	4–24	170–1150
800	3600–5400	6–38	340–2400

compact with 0.3–2.0 μm pore size (x in Equation 3), a capillary pore radius of 0.265 μm (a in Equation 3) and a surface tension of borosilicate glass of 0.3 $N m^{-1}$ [22] was then calculated using Equation 3. The results of these calculations are shown in Table III under the heading of Equation 3, along with the measured times to reach the constant densification factor, which are assumed as the measured infiltration times. It is noted that the calculated values are one to two orders of magnitude lower than the measured values, indicating that the densification mechanism can not be described by glass redistribution kinetics based on time-independent contact angle alone.

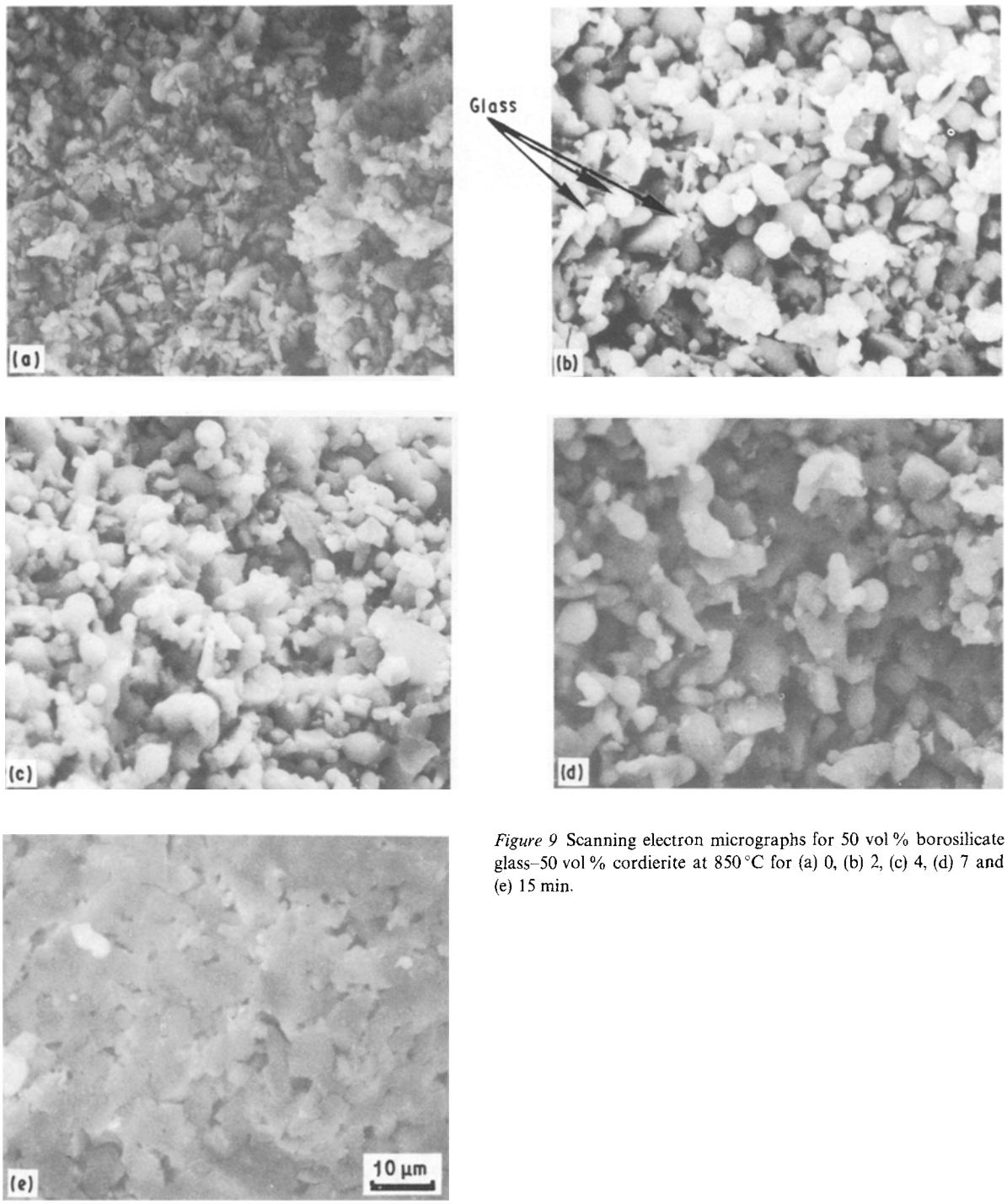

Figure 9 Scanning electron micrographs for 50 vol % borosilicate glass–50 vol % cordierite at 850 °C for (a) 0, (b) 2, (c) 4, (d) 7 and (e) 15 min.

This discrepancy has led us to consider a time-dependent contact angle. Strong support for this approach came from microstructural observations. A careful examination of the microstructure of the sintered composite as a function of time (Fig. 9) revealed that the sintering proceeds by an initial transformation of melted glass into spheres, followed by the spreading of the melt into the pores. Note that the starting glass powder (Fig. 9a) has an irregular shape. As the sintering proceeds (Fig. 9b), under the influence of surface tension the glass powder suddenly forms an array of spheres to minimize their volume free energy. However, with continued sintering (Fig. 9c–9e) the system further lowers its volume free energy as lower energy solid–liquid interfaces are created (i.e. the glass wets the cordierite) at the expense of higher energy solid–vapour, and melt–vapour interfaces. This causes the glass to spread out and redistribute itself into the pores, yielding shrinkage and densification. These observations indicate that under the sintering conditions investigated, the contact angle of glass decreases with time for reasons still not entirely clear, and that the kinetics of melt redistribution will be affected by this time-dependent wetting behaviour. It is, however, recognized that the time-dependent wetting behaviour may also arise as a result of a limited chemical reaction between the glass and the cordierite, the evidence of which was not readily available from EDX. Another possibility is that an unknown surface layer responsible for temporary dewetting may have formed/retained during initial period of heating, and that this layer disappears during further heating. Clearly this area requires further studies.

The problem then was to determine a time-dependent contact angle between borosilicate glass and the cordierite. As stated earlier, the contact angle appeared to reach its equilibrium value instantly at the experimental temperatures from 800–900 °C by using glass powder on cordierite. The time-scale of the experiment did not allow us to observe the time-dependent wetting behaviour with glass powder. It was, however, found that by increasing the size of the glass powder, the phenomenon could be observed on an experimental time scale. Because the contact angle should only be a function of relative interfacial energies and not of particle size, the origin of this time-dependent contact angle with large glass particle sizes must be attributed to kinetics such as those discussed earlier. To measure non-equilibrium time-dependent contact angle, the glass powder was first pressed, sintered at 900 °C for 240 min, cooled and broken to pieces of approximately $10 \times 10 \times 5\,mm^3$ and irregular shapes. The glass pieces thus prepared were then heated on the cordierite or fused silica substrates to measure the time-dependent contact angle. The examples of several time-dependent contact-angle measurements are shown in Fig. 10 for cordierite and fused silica substrates. For comparison, the results reported by Tummala and Foster [22] using borosilicate glass on 99.5% alumina are also presented in the figure. Note that they also observed a time-dependent contact angle. It appears from this comparison that the time-dependent contact angle is substrate-dependent. Secondly, the time-dependent contact angle starts with a larger value, then approaches the equilibrium contact angle slowly with time. The two sets of measurements on cordierite substrates are almost identical, although a higher starting value is obtained for a different set of measurements. This variation is believed to be due to different geometry of glass and different surface characteristics of the substrates. However, the rate at which the contact angle decreases appears to remain the same. Note also that the measured contact angles using glass powder on cordierite are generally smaller than those using glass pieces at the same temperature, probably because the powder is more reactive due to its higher surface energy.

An empirical equation proposed by Newman [23] to describe the contact angle as a function of time, and can be expressed as

$$\cos\theta_t = (1 - \alpha e^{-\beta t})\cos\theta_\infty \quad (4)$$

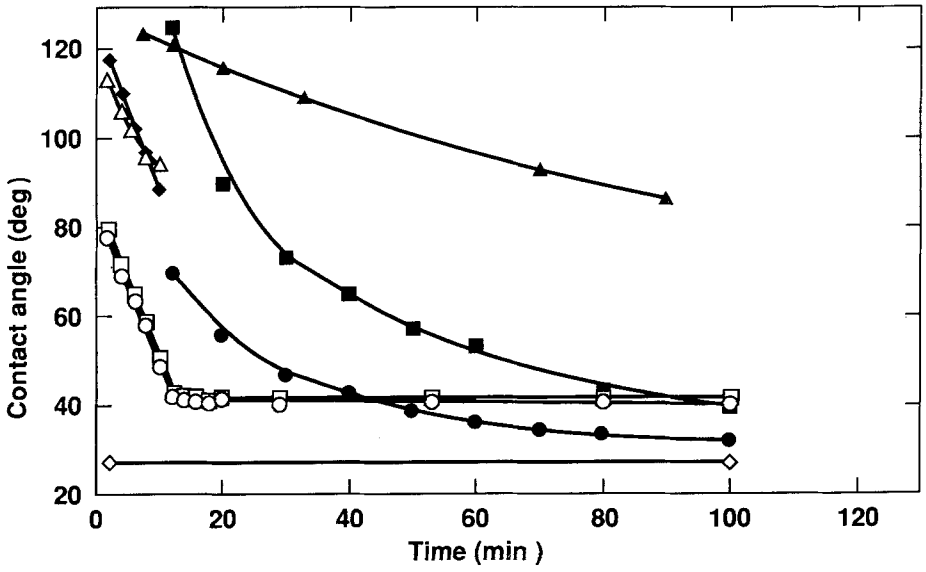

Figure 10 Contact angle of borosilicate glass on various substrates at 900 °C (BS = borosilicate glass). (▲) BS/silica in air, (■) BS/alumina in dry nitrogen [22], (●) BS/alumina in wet nitrogen [22], (◆, △, □, ○) BS/cordierite in air, (◇) BS powder/cordierite in air.

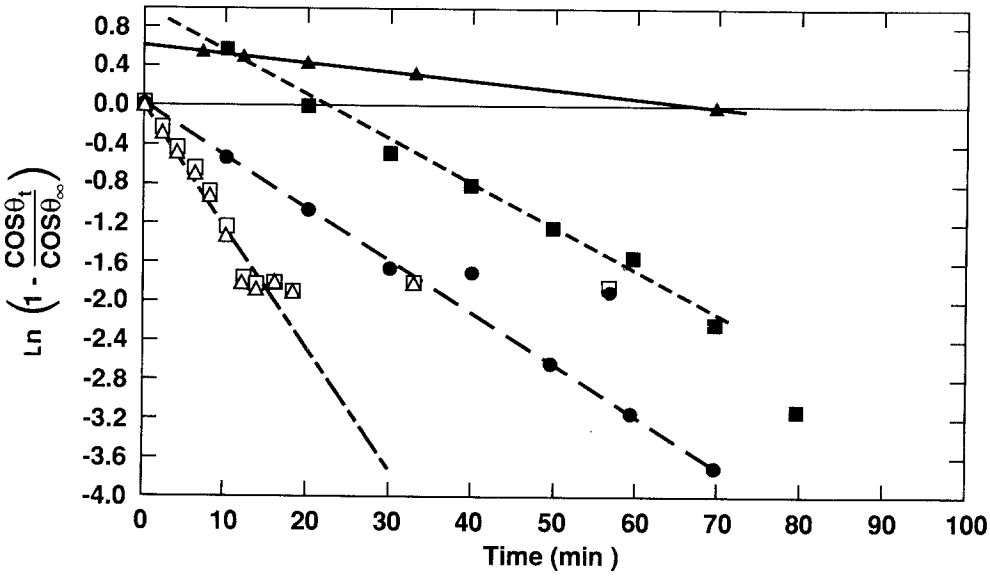

Figure 11 Ln(1-cosθ_t/cosθ_∞) versus time for borosilicate glass on various substrate at 900 °C (BS = borosilicate glass). (▲) BS/silica, (■) BS/alumina in dry nitrogen [22], (●) BS/alumina in wet nitrogen [22], (□ △) BS/cordierite.

where θ_t is the instantaneous contact angle, and α and β are constants. α will be 1 if $\theta = \pi/2$ when $t = 0$. β is related to the surface tension and viscosity of the melt, and is given [23] by

$$\beta = k\gamma/\eta \quad (5)$$

where k is a constant. Note that β is system-dependent and inversely proportional to the viscosity of melt because the surface tension is generally insensitive to temperature. Inserting Equations 4 and 5 into Equation 3 and using fluid mechanics, the infiltration distance can be expressed as follows [24–28]

$$x^2 = \frac{\gamma a \cos\theta_\infty}{2\eta}\left(t - \frac{1}{\beta} + \frac{e^{-\beta t}}{\beta}\right) \quad (6)$$

For using Equation 6 to calculate the infiltration time, the value of β must be known. Replotting the data shown in Fig. 10 as $\ln(1 - \cos\theta_t/\cos\theta_\infty)$ versus time, as shown in Fig. 11, the beta value can be determined from the slope of the linear portion by a least-squares fit method. It is found that the β at 900 °C is 2.32 $\times 10^{-3}$ s^{-1} for the borosilicate glass on the cordierite. The values for β at different temperatures were then calculated using Equation 5 and the viscosity data in Table I. They are as follows: 1.23×10^{-3} s^{-1} at 875 °C, 0.62×10^{-3} s^{-1} at 850 °C, 0.29×10^{-3} s^{-1} at 825 °C, and 0.14×10^{-3} s^{-1} at 800 °C. For comparison, the β values for those results obtained by Tummala and Foster [22] are also calculated to be 8.42×10^{-4} s^{-1} for borosilicate glass on alumina in wet nitrogen and 6.66×10^{-4} s^{-1} in dry nitrogen at 900 °C. The β value on silica is 1.97×10^{-5} s^{-1} at 900 °C in this study.

The time needed for borosilicate glass to infiltrate a porous compact with a 0.3–2.0 μm pore size (x in Equation 6) can now be calculated using Equation 6 for time-dependent contact angle. Using the same capillary pore size, 0.265 μm (a in Equation 6), and surface tension of borosilicate glass as for time-independent contact-angle case, the calculated results are shown in Table III under the heading of Equation 6. Note that the infiltration times calculated by Equation 6 are one to two orders of magnitude larger than those calculated by Equation 3 and are of the same order of magnitude as the measured time periods needed to reach constant densification factor. The deviation from the measured values can be readily accounted for by recognizing that there exists a distribution of pores in the sample from 0.3–2 μm as stated before. Furthermore, we recognize the limitation that our contact angle–time measurement cannot exactly simulate the microstructural observation of the time-dependent wetting behaviour which is observed with glass powder. In spite of this, the combined observations of densification factor–time curves (Figs 2 and 3), the microstructural evolution (Fig. 9), and the contact angle–time data (Fig. 10) provide strong support to the following conclusions: that the time-dependent contact-angle kinetics should be considered in estimating the redistribution period, and that the glass-redistribution kinetics can be reasonably estimated by that of melt infiltration into a porous compact with an equivalent pore size.

5. Conclusions

Densification kinetics and mechanisms of borosilicate glass-filled cordierite ceramics have been analysed by using densification rate, microstructure, and infiltration behaviour of melt into the porous structure. It is found that the densification and the densification rate increase with increasing sintering temperature and glass content. Microstructural observations show that the densification of borosilicate glass-filled cordierite system at 800–900 °C is achieved mainly in the initial stage of liquid-phase sintering. The apparent activation energies of densification, 330–390 kJ mol^{-1}, remain unchanged with glass content ranging from 30–60 vol %, and are close to that of viscous flow of the borosilicate glass, 290–310 kJ mol^{-1}. These results suggest that the densification is controlled by the

viscous flow of glass. However, it is found that the densification results cannot be solely interpreted by viscous sintering of glass, and that the redistribution of the glass melt between cordierite particles should be considered. Based on microstructural observations, it is seen that as the sintering proceeds, the glass exhibits an initial dewetting with respect to cordierite, which is then followed by a complete wetting of the cordierite by the glass. This suggests that the time-dependent contact angle between the melt and the solid plays a significant role in the glass-redistribution process. It is speculated that this may arise either from a limited chemical reaction between the glass and the cordierite or from the elimination of impurities at the glass/cordierite interface as the sintering proceeds. The redistribution time calculated from a time-dependent contact angle is in good agreement with the time required for sintering to reach a constant densification factor.

Acknowledgements

The authors thank Professor Gary Messing, Pennsylvania State University, for reviewing the manuscripts and providing many valuable suggestions. The contributions of C. Sell, A. Wertz and K. Tipinski are appreciated. We also thank Professor W. C. LaCourse, Alfred University, for glass viscosity measurements.

References

1. H. S. CANNON and F. V. LENEL, in "Proceedings of the Plansee Seminar", edited by F. Benesovsky (Metallwerk Plansee, Reutte, 1953) p. 106.
2. W. J. HUPPMANN and G. PETZOW, in "Sintering Process", edited by G. C. Kuczynski (Plenum Press, New York, 1980) p. 189.
3. W. J. HUPPMANN and G. PETZOW, *Ber. Bunsenges Phys. Chem.* **82** (1978) 308.
4. R. M. GERMAN, in "Liquid Phase Sintering" (Plenum Press, New York, 1985) Ch. 4.
5. J. H. JEAN and C. H. LIN, *J. Mater. Sci.* **24** (1989) 500.
6. R. M. GERMAN, in "Liquid Phase Sintering" (Plenum Press, New York, 1985) Ch. 4.
7. V. N. EREMENKO, Y. V. NAIDICH and I. A. LAVRINENKO, in "Liquid Phase Sintering" (Consultants Bureau, New York, 1970) Ch. 4.
8. K. V. SEBASTIAN and G. S. TENDOLKAR, *Powder Metall. Int.* **11** (1979) 62.
9. W. D. KINGERY, E. NIKI and M. D. NARASIMHAN, *J. Amer. Ceram. Soc.* **44** (1961) 29.
10. K. G. EWSUK, L. W. HARRISON and F. J. WALCZAK, in "Ceramic Transations", Vol. 1, edited by G. L. Messing, E. R. Fuller and H. Hausner Jr (American Ceramic Society, Westerville, 1988) p. 969.
11. K. S. HWANG, PhD thesis, Rensselaer Polytechnic Institute, Troy (1984).
12. J. W. CAHN and R. B. HEADY, *J. Amer. Ceram. Soc.* **53** (1970) 406.
13. W. J. HUPPMANN and H. RIEGGER, *Acta Metall.* **23** (1975) 965.
14. J. SZEKELY, in "Fluid Flow Phenomena in Metals Processing" (Academic Press, New York, 1979) Ch. 1.
15. Y. V. NAIDICH, I. A. LAVRINEMKO and V. A. EUDOKIMOV, *Sov. Powder Metall. Met. Ceram.* **13** (1974) 26.
16. W. D. KINGERY, *J. Appl. Phys.* **30** (1959) 301.
17. O. H. KWON, PhD thesis, Pennsylvania State University (1986).
18. J. FRENKEL, *J. Phys. (USSR)* **IX** (1945) 385.
19. J. K. MACKENZIE and R. SHUTTLEWORTH, *Proc. Phys. Soc. Lond. B* **62** (1949) 833.
20. G. W. SCHERER, *J. Amer. Ceram. Soc.* **60** (1977) 236.
21. S. PEJOVNIK, D. KOLAR, W. J. HUPPMANN and G. PETZOW, in "Sintering – New Developments", edited by M. M. Ristic (Elsevier Scientific, Amsterdam, Netherlands, 1979) p. 285.
22. R. R. TUMMALA and B. J. FOSTER, *J. Mater. Sci. Lett.* **10** (1975) 905.
23. S. NEWMAN, *J. Colloid Interface Sci.* **26** (1968) 209.
24. D. H. R. SARMA, PhD thesis, Purdue University (1982).
25. R. A. GREENKORN and D. P. KESSLER, in "Transfer Operations" (McGraw-Hill, New York, 1972) p. 59.
26. I. H. SHAMES, in "Mechanics of Fluids" (McGraw-Hill, New York, 1962) p. 94.
27. J. R. LIGENZA and R. B. BERSTEIN, *J. Amer. Chem. Soc.* **73** (1951) 4636.
28. J. SZEKELEY, A. W. NEUMANN and Y. K. CHUANG, *J. Colloid Interface Sci.* **35** (1971) 273.

Received 15 November 1990
and accepted 20 March 1991